Geophys. J. Int. (2003) **155,** 308–318

Anomalous phases exceeding 90° in magnetotellurics: anisotropic model studies and a field example

Wiebke Heise and Jaume Pous

Departament de Geodinàmica i Geofísica, Universitat de Barcelona Martí i Franquès s/n, 08028 *Barcelona, Spain. E-mail: wiebke@geo.ub.es*

Accepted 2003 May 21. Received 2003 May 21; in original form 2002 September 30

SUMMARY

A study of synthetic anisotropic models that explain phases exceeding 90° in magnetotellurics is presented. The basic model comprises an anisotropic layer overlain by a shallow (local) anisotropic block, with both structures inserted in a 2-D model. The 2-D strike and the anisotropy strikes (layer and block) differ. The influence of the following parameters was analysed: anisotropy strike, geometry of the block and the layer, and anisotropy ratios of the block and the layer. We show that, according to this model, the anomalous phase effect is limited to those sites above the shallow block and does not influence the regional structure, which can therefore be recovered. These results were applied to field data from a magnetotelluric profile in SW Iberia where phases greater than 90° occurred in an area in which alternating bands of schist and graphite-rich blackschists crop out, giving rise to strong macroanisotropy.

Key words: anisotropy, electrical conductivity, magnetotellurics, phases.

INTRODUCTION

Large phase anomalies, in particular those exceeding 90°, are sometimes observed in magnetotelluric (MT) surveys. However, as they are little understood and cannot be modelled by standard 1-D and 2-D methods, they are usually excluded from inversion procedures. These anomalies are usually considered to be galvanic distortions caused by a strong channelling of electric currents, the current channelling. The impedance phase describes the phase shift between the components of the electric field **E** and the magnetic field **H**. It is given by $\varphi_{ij} = \arctan(\mathrm{Im}\ Z_{ij}/\mathrm{Re}\ Z_{ij})$ (i, j refers to the three axes x, y, z), where Z_{ij} are the complex elements of the second-order impedance tensor $\boldsymbol{Z}$, which defines the linear relation between the electric and magnetic fields as $\mathbf{E} = \boldsymbol{Z}\mathbf{H}$. $\boldsymbol{Z}$ contains information on the conductivity of the Earth. As a result of the principle of causality of the interaction between electric and magnetic fields induced in the Earth the phases should lie in the first or third quadrant [0°; 90°]; [180°; 270°]. This implies that the imaginary and real impedance have the same sign. However, Egbert (1990) shows that the principle of causality can be violated by certain physically realizable 3-D conductivities. He demonstrated this empirically with a model of a sharp channelling body (a conductive sheet broken with resistive lines embedded in a perfect resistive layer), which results in a reverse of the direction of the electric field, while the magnetic field remains nearly constant. With this model a distortion effect (phases greater than 90°) observed at some sites of the EMSLAB data set (EMSLAB Group 1988) were reproduced.

Recently, several attempts have been made to model large phase anomalies using current channelling structures. Livelybrooks *et al.* (1996) explained a large phase anomaly found in a survey across the Trillabelle ore body (Sudbury, Ontario) with 3-D induction within the body coupled with current channelling through neighbouring faults. Lezaeta (2001) explained phases greater than 90° observed in the Andes at the Precordillera and the coast with models of near-surface elongated 3-D conductors being electromagnetically coupled with a conductive ocean and conductive mantle, producing strong current channelling and magnetic distortions. Weckmann (2002) modelled phases greater than 90° in a survey in Namibia with a conductive local ring-structure and Pous *et al.* (2002) attempted to model more regional large phase anomalies found in Tenerife island using 3-D, highly conductive, channel structures.

Pek & Verner (1997) have suggested that a combination of two azimuthal anisotropies with anisotropy strikes perpendicular to each other could also produce phases that exceed 90°. In a recent MT survey carried out in SW Iberia, phases much greater than 90° were found at a number of sites located in a formation in which subvertical alternating bands of schists and blackschists with a high content of well-interconnected graphite crop out (Pous *et al.* 2003), and in which macroscopic anisotropy occurs. Using the model proposed by Pek & Verner (1997) as the basis of our study, we vary the model parameters in order to determine the conditions under which the anomalous phases appear. We found that this model fits the anomalous data from the MT survey conducted in SW Iberia and that it was consistent with the geology.

SYNTHETIC DATA

Fig. 1(a) defines the azimuthal anisotropy simulated by subvertical sheets where the principal resistivities are $\rho_{\min}/\rho_{\max}$. The anisotropy strike α is measured with respect to the 2-D strike of the background

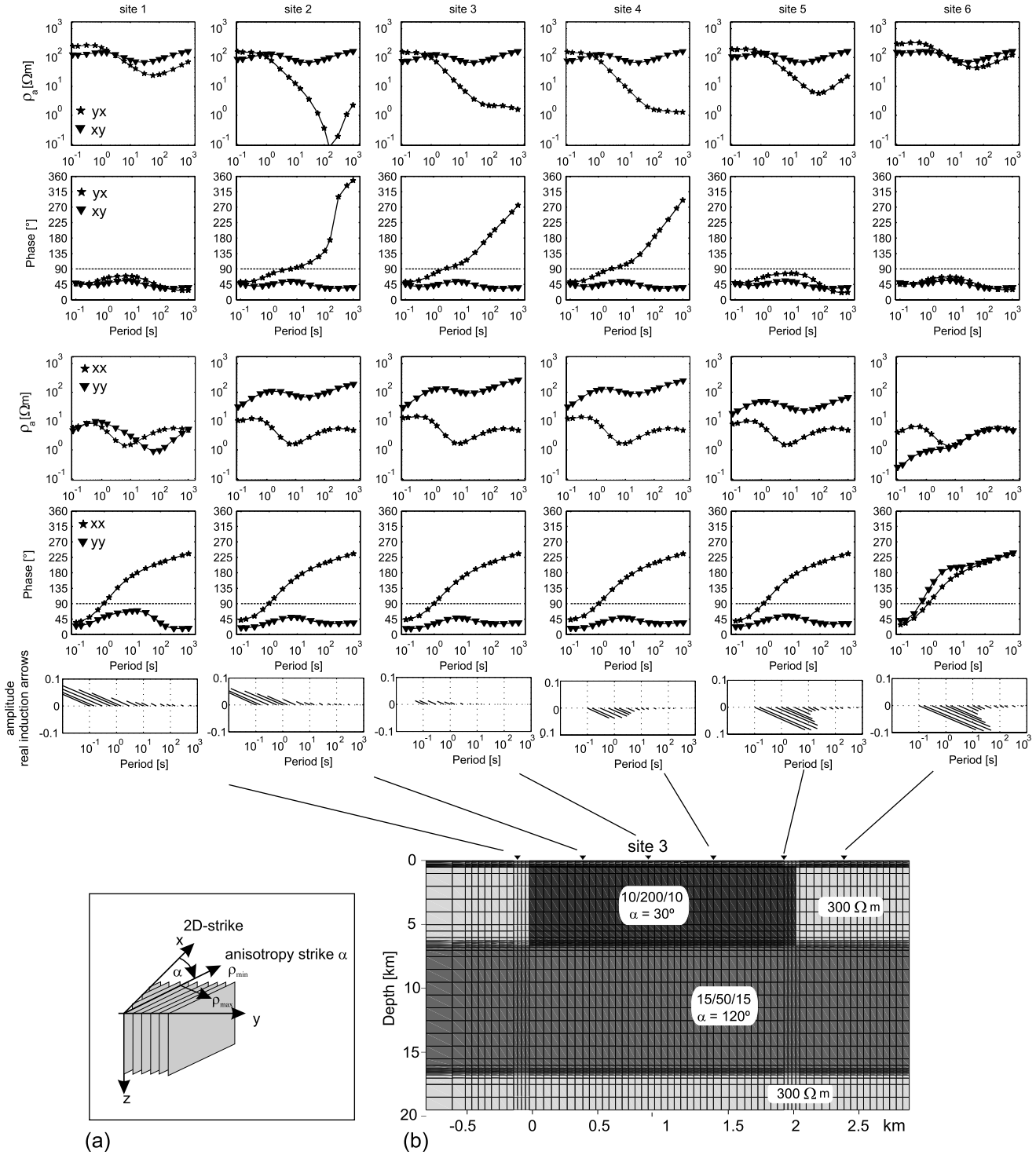

Figure 1. (a) An azimuthal anisotropic domain with the principal resistivities $\rho_{\min}$ and $\rho_{\max}$. $\rho_{\min}$ lies along the anisotropy strike α and $\rho_{\max}$ perpendicular. (b) The initial model and responses.

isotropic 2-D model. The initial model (Fig. 1b) consists of a narrow anisotropic block striking 0° starting at a depth of 350 m embedded in a medium of 300 Ω m. The principal resistivities of the block are $\rho_{\min}/\rho_{\max} = 10/200$ Ω m and the anisotropy strike α is 30°. The block is underlain by an anisotropic layer with principal resistivities 15/50 Ω m and an anisotropy strike of 120° (perpendicular to α of the block). The anisotropic layer is underlain by a 300 Ω m half-space. The responses were calculated using the finite-difference code for 2-D models with arbitrary anisotropy of Pek & Verner (1997). The dimensions of the grid were 99 × 70 (horizontal × vertical) including 10 air layers. The mesh elements are shown in Fig. 1(b): in the y direction the cell spacing over the block was

between 60 and 30 m, while in the z direction it was 50 m at the upper boundary of the block and 125 m at the boundary between the block and the layer.

In Fig. 1(b) we see the four components (x and y axes) of apparent resistivities and phases along a profile crossing the block. The phases of the yx component at sites above the block leave the quadrant, reaching values higher than 200°, while the corresponding branches of the apparent resistivity curves (yx) descend steeply. At sites within the block but very close to the contact the effect disappears (site 5). Note that the xx component has phases higher than 90° at all the sites, even at a distance from the shallow block. This is normal behaviour for the responses of 2-D (even isotropic) models in a coordinate system different from the 2-D strike direction.

Fig. 2 shows the pseudosections of the yx component of apparent resistivity and phase calculated in each element of the mesh along the profile. The phases greater than 90° occur within the whole block, with the exception of points near the edges. Resistivities are very low across the block, the minimum values being near the edges. This anomalous behaviour of the phases exceeding 90° is a consequence of the tensorial character of conductivity in an anisotropic medium. It is well known that the phase component of the electric field perpendicular to the conductivity contrasts is not continuous throughout the contacts. The current density is not parallel to the electric field and in some conductivity structures both the current density and the electric field can almost be reversed within a near-surface section of the anisotropic shallow block (Pek & Verner 1997). If the shallow anisotropic block outcropped, the anomalous phases would extend over the whole block. The overburden smooths the jump in the boundaries of the block and therefore no anomalous phases occur at sites near the boundaries within the block (e.g. site 5, Fig. 1).

At sites near the edges of the block the real induction arrows (Wiese convention, pointing away from high conductivity zones) point approximately perpendicular to the anisotropy strike (30°) of the block (Fig. 1b). Over the block and at some distance from the contacts, the arrows are very small, because horizontal anisotropic layers induce no vertical magnetic field. However, in anisotropic media the directions of the induction arrows are highly sensitive to changes in the resistivity contrasts of the model (Weidelt 1999). Therefore, the induction arrows may show distinct behaviour if we consider more complicated models including more conductors.

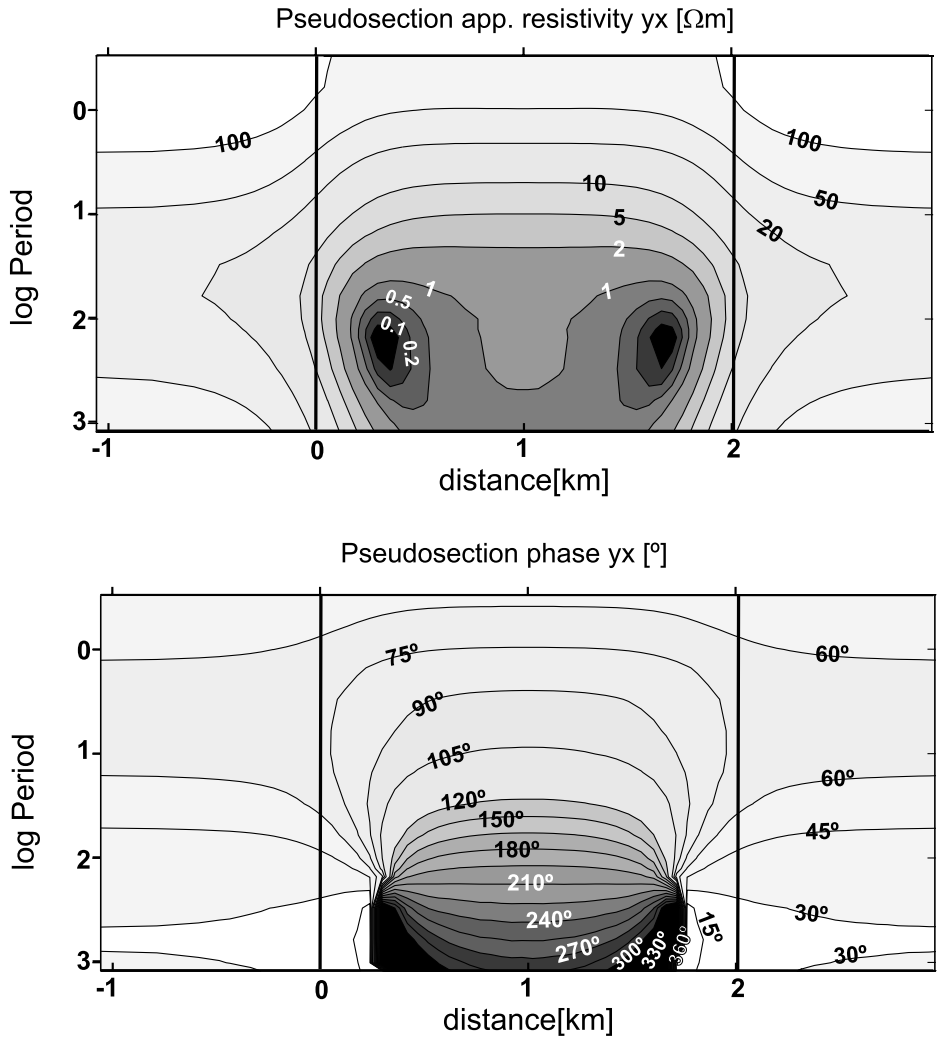

Figure 2. Pseudosections of the yx-component of apparent resistivities and phases. The vertical black lines denote the lateral boundaries of the anisotropic block.

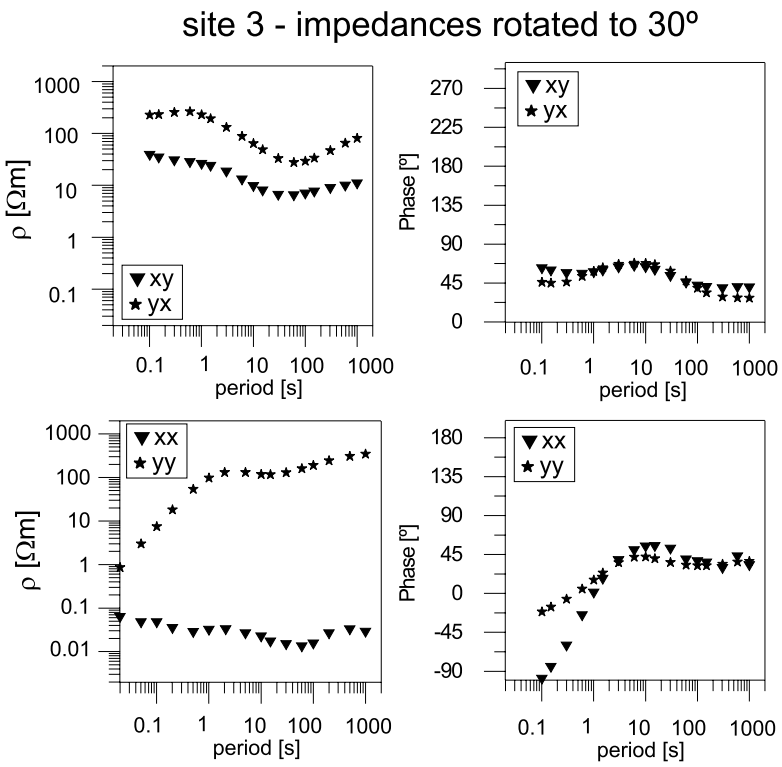

Figure 3. The four components of apparent resistivities and phases at site 3 for the impedance tensor rotated by 30°. Note that at this angle the phases of the *yx* component do not leave the quadrant.

The coordinate system of the measurement

The responses of Fig. 1(b) correspond to the impedance tensor measured in the direction of the 2-D isotropic strike (axes x, y: x is aligned with the 2-D strike). However, this effect (phases higher than 90°) depends on the coordinate system of measurement, so it vanishes when approaching the direction of the anisotropy strike of the block (α). In Fig. 3 we show for site 3 the four components of the impedance tensor rotated to the anisotropy strike of the block (30°). Note that for this coordinate system (rotation angle of 30°) the effect on the phases vanishes in the *yx* mode. The diagonal element *xx* of the apparent resistivities becomes very small, although the *yy* component remains high. The phases out of quadrant at short periods of the *xx* polarization mode appear because the coordinate system is different from the 2-D isotropic strike direction. At short periods, 30° is the direction at which the modulus of the diagonal elements are at their smallest and, therefore, the Swift criterion gives the anisotropy strike of the block as the local 2-D strike direction (Heise & Pous 2001).

Influence of the model parameters

In the following we analyse the sensitivity of the responses to variations in the model parameters. The parameters analysed are: the direction of the anisotropy strikes, the anisotropy contrast $\rho_{\min}/\rho_{\max}$, the geometry (depth, thickness, width) of the block and the angle between anisotropy strikes of the block and the layer.

Anisotropy strike of the block

Fig. 4(a) shows the behaviour of the four components of apparent resistivities and phases when varying the anisotropy strike of the block while the anisotropy strike of the layer is kept perpendicular to that of the block. Up to periods of about 150 s the *yx* phases increase continuously with α, reaching their maximum (around 180°) when $\alpha = 40°$. When $\alpha > 40°$, the phases decrease with α. At periods longer than 150 s there is a discontinuity in this sequence: for α around 20° and 60°, the phases ascend very steeply up to 360°. The apparent resistivities for these cases have a marked minimum at about 200 s (corresponding to 180° in the phase curve) and thereafter they increase again. Note the violation of the dispersion relations between apparent resistivity and phase (Berdichevsky 1999) occurring at these longer periods. In contrast, the other three components have a more regular sequence in which the phases increase continuously with α throughout the whole period range.

Anisotropy ratio of the block

Phases higher than 90° appear only when the anisotropy ratio (contrast $\rho_{\min}/\rho_{\max}$) of the block is high. In Fig. 4(b) we see, starting with a maximum contrast of $\rho_{\min}/\rho_{\max} = 10/200\ \Omega$ m, that the effect of the *yx*-phases decreases continuously as the anisotropy ratio falls. A discontinuity in this sequence also appears at periods higher than 150 s when the ratio is around $20/200\ \Omega$ m. Note that the curves present the same behaviour as in the above case.

Depth of the top of the anisotropic block

The depth of the top of the anisotropic block was successively increased, while its bottom was kept at the same depth. The large phase effect decreases with the depth of the block (Fig. 4c). At depths greater than 800 m the phases do not exceed 90°. At short

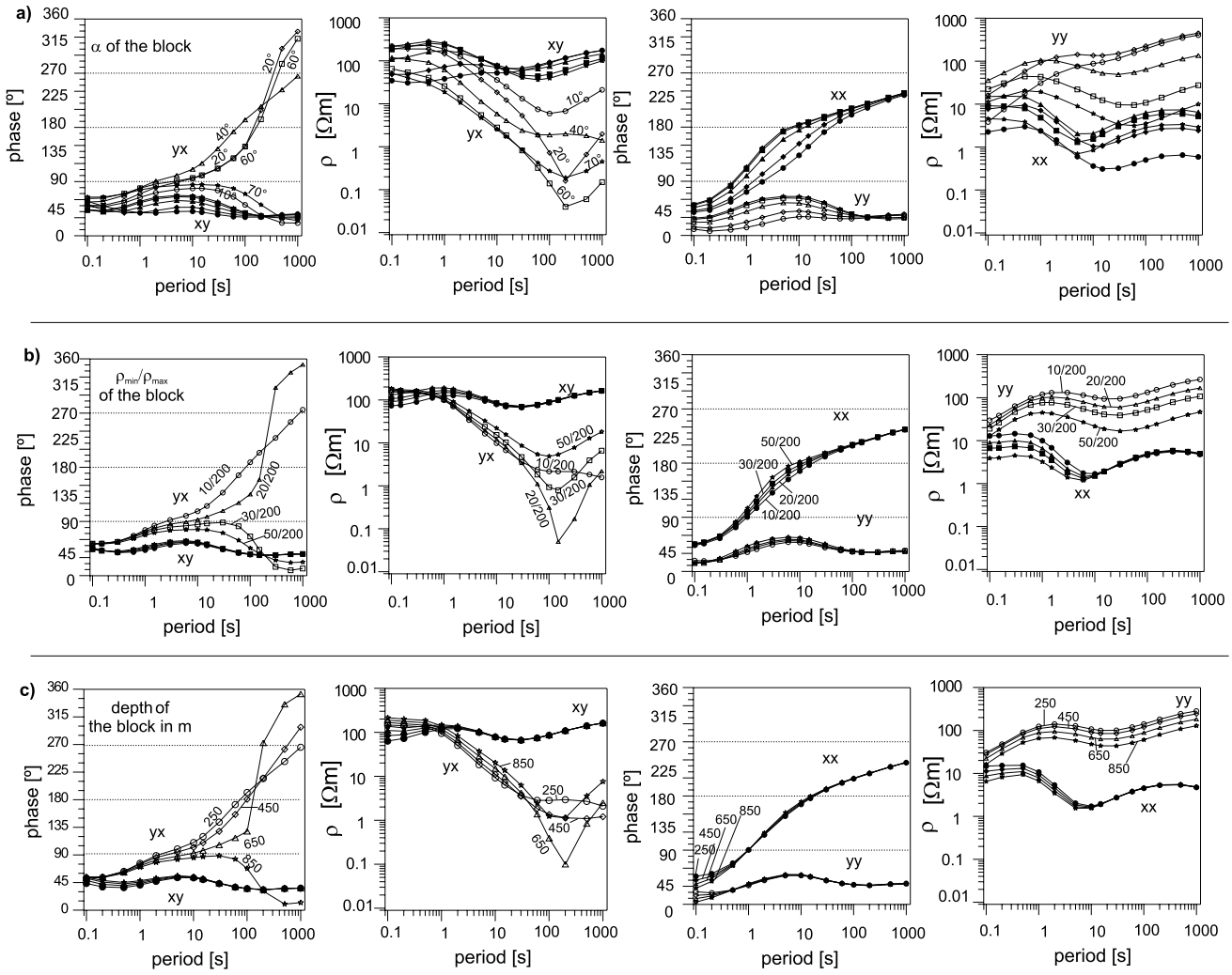

Figure 4. Phases and apparent resistivities when varying model parameters at site 3 in the coordinate system of the 2-D isotropic strike (0°): (a) for different anisotropy strikes α; (b) for different anisotropy ratios of the block; (c) for different depths of the top of the anisotropic block. Note the discontinuity in the sequences at periods longer than 150 s and cases where $\alpha = 20°$, $60°$, $\rho_{\min}/\rho_{\max} = 20/200$, depth = 650 m.

periods, up to 150 s, the phase and resistivity curves show the typical behaviour for the *yx*-phases and apparent resistivities, whereas at periods longer than 150 s, a discontinuity once again occurs in the sequence when the top of the block is around 650 m. Because of the induction character, increasing the depth of the block is equivalent to decreasing the resistivity of the overburden.

Anisotropy ratio of the layer

The higher the anisotropic ratio (i.e. the greater the contrast $\rho_{\min}/\rho_{\max}$) of the layer the greater the effect on the data. Indeed, high anisotropic ratios of the layer produce phases higher than 90° even with an anisotropic ratio of the block lower than 20/200 Ω m.

Angle between anisotropy strikes

For this model, the angle between anisotropy directions of the block and the layer must be higher than 70° to obtain phases out of quadrant. The maximum phases appear when both anisotropy directions are perpendicular.

Thickness of the block

The thickness of the block was reduced continuously from the 6.5 km of the base model (Fig. 1b), so that the layer and the block were no longer connected. We found phases higher than 90° as long as the block had a thickness of up to 1000 m, demonstrating that this behaviour is caused by a local structure.

Width of the block

A further limiting factor for the anomalous phases is the width of the block. We found that for block widths between 700 m and 7 km phases out of quadrant did occur. However, for great block widths the effect decreased at sites in the centre of the block, away from the margins.

The behaviour of the curves when varying these parameters was very similar (Fig. 4). This means that there is an ambiguity in the determination of the model parameters. For instance, the phase *yx* curve for $\alpha = 20°$ and for an anisotropy ratio of 10/200 Ω m (Fig. 4a) is the same as that for the model with $\alpha = 30°$ and an anisotropy

ratio of 20/200 Ω m (Fig. 4b). Only by using the four components of the impedance tensor can the ambiguity be reduced.

MEANING OF THESE ANOMALOUS PHASES

The impedances

Phases in the second and fourth quadrant ([90°; 180°] and [270°; 360°]) mean that the imaginary and real impedance have different signs. Fig. 5 shows the *yx* impedance components corresponding to different cases of Fig. 4. Fig. 5(a) corresponds to anisotropy strikes of the block of 10°, 20° and 40°. In the case $\alpha = 10°$, the real and imaginary impedances have the same sign for all periods, thus the phases do not reach 90°. When $\alpha = 20°$ the real part of the impedance is positive, whereas the imaginary part is negative in the period range of 10–100 s. Accordingly, the phases lie between 90° and 180°. At 150 s the imaginary part also becomes positive and the phases are higher than 180°. At this period both imaginary and real impedances become very small and, therefore, the *yx*-apparent resistivity becomes extremely low. At longer periods, the real part again passes zero to become negative and the phases lie between 270° and 360°. The third case, $\alpha = 40°$, is similar but at the longest periods both real and imaginary parts maintain the same sign and, therefore, the *yx* phases remain in the third quadrant. Similar behaviour occurs in Fig. 5(b) when varying the anisotropy ratio of the block, and in Fig. 5(c) when varying the depth of the top of the shallow block. Note that in the three panels of the second column ($\alpha = 20°$, $\rho_{min}/\rho_{max} = 20/200$, depth of the block 650 m) both real and imaginary impedances cross zero simultaneously (at around 150 s). Thus, a very low apparent resistivity and an extreme slope of the phase curves occur at around this period (see Fig. 4). This is the reason for the discontinuity in the sequence when varying the model parameters in Fig. 4.

Thus, when varying the model parameters we always find between the range of parameter values producing normal phases (<90°) and

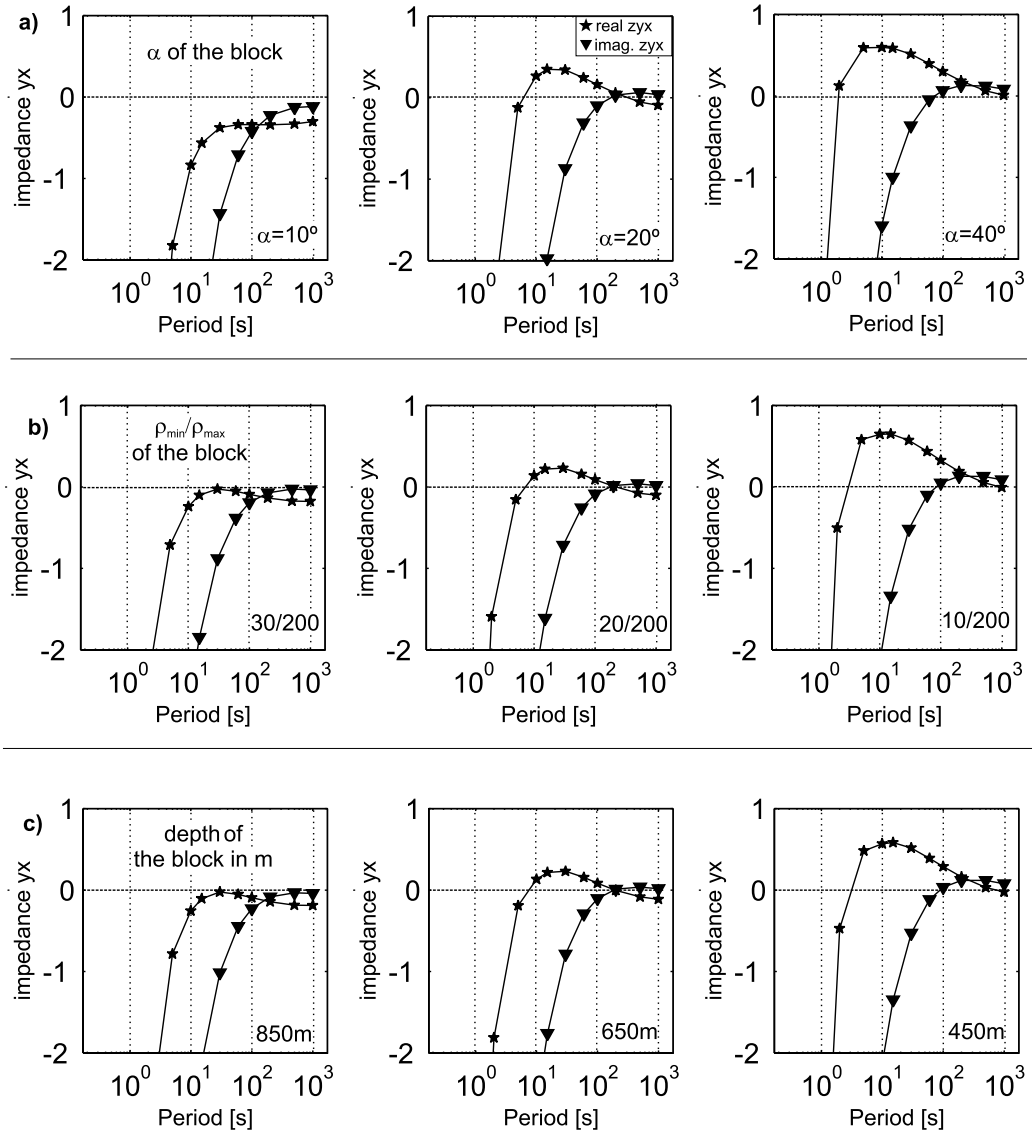

Figure 5. Real and imaginary part of the *yx* impedances of site 3 when varying the anisotropy strike α (a), the anisotropy contrast (b) and the depth of the top of the block (c).

the range of parameter values producing anomalous phases (>90°) a narrow range of parameters with highly anomalous behaviour (e.g. $\alpha = 20°$, $\rho_{\min}/\rho_{\max} = 20/200$, depth of the block = 650 m). Note that these zones of highly anomalous behaviour also occur near the edges of the block of the base model (see pseudosections, Figs 2 and 1, site 2).

The electric field

There is an easy way to see such behaviour in terms of the electric field. Let us assume two perpendicular polarizations of the primary magnetic field, $H_{py}^{(1)} = 1$, $H_{px}^{(1)} = 0$ and $H_{py}^{(2)} = 0$, $H_{px}^{(2)} = -1$. Then the impedance element Z_{yx} is given by

$$Z_{yx} = \frac{E_y^{(1)} H_y^{(2)} - H_y^{(1)} E_y^{(2)}}{H_x^{(1)} H_y^{(2)} - H_y^{(1)} H_x^{(2)}} = \frac{H_y^{(2)}}{H_y^{(1)}} E_y^{(1)} - E_y^{(2)}. \quad (1)$$

If $H_x^{(1)} \equiv 0$ and $H_x^{(2)} \equiv -1$ is considered. $[H_y^{(2)}/H_y^{(1)}]\, E_y^{(1)}$ becomes very small (for our model and a broad range of resistivity contrasts in the anisotropic model) and we can neglect the first term and set $Z_{yx} \approx -E_y^{(2)}$ without a loss of generality in the following (Pek, private communication, 2003). Fig. 6 shows the electric field components for the $H_{py}^{(2)} = 0$, $H_{px}^{(2)} = -1$ polarization of the primary magnetic field, plotted across the anisotropic block at 10, 150 and 500 s for the cases $\rho_{\min}/\rho_{\max} = 10/200$ and $\rho_{\min}/\rho_{\max} = 20/200$. The parallel electric field E_x is not affected by the anisotropic block, whereas the transverse electric field E_y is strongly distorted by the anisotropic block. From the boundary conditions $j_y^{\mathrm{h}} = j_y^{\mathrm{b}}$ (continuous currents through the contact host medium–block) applying Ohm's law we obtain $\boldsymbol{\sigma}^{\mathrm{h}}\, E_y^{\mathrm{h}} = \boldsymbol{\sigma}_{xy}^{\mathrm{b}}\, E_x + \boldsymbol{\sigma}_{yy}^{\mathrm{b}}\, E_y^{\mathrm{b}}$. The transverse electric field over the block is then

$$E_y^{\mathrm{b}} = \frac{\boldsymbol{\sigma}^{\mathrm{h}}}{\boldsymbol{\sigma}_{yy}^{\mathrm{b}}} E_y^{\mathrm{h}} - \frac{\boldsymbol{\sigma}_{xy}^{\mathrm{b}}}{\boldsymbol{\sigma}_{yy}^{\mathrm{b}}} E_x, \quad (2)$$

where b denotes the anisotropic block and h denotes the isotropic host medium. The first term of formula (2) $(\boldsymbol{\sigma}^{\mathrm{h}}/\boldsymbol{\sigma}_{yy}^{\mathrm{b}})\, E_y^{\mathrm{h}}$ is the scaling by the ratio of the conductivities on either side of the contact. In the anisotropic media the conductivity is described by a tensor and an additional term $(\boldsymbol{\sigma}_{xy}^{\mathrm{b}}/\boldsymbol{\sigma}_{yy}^{\mathrm{b}})E_x$ occurs, which can easily grow very large, even larger than the first term and then the transverse electric field can have a reversed orientation within the block. The ratio $\boldsymbol{\sigma}_{xy}^{\mathrm{b}}/\boldsymbol{\sigma}_{yy}^{\mathrm{b}}$ depends on the anisotropic ratio and on the anisotropic strike: $\sigma_{xy}^{\mathrm{b}} = (\sigma_{\max}^{\mathrm{b}} - \sigma_{\min}^{\mathrm{b}})\sin\alpha\, \cos\alpha$ and $\sigma_{yy}^{\mathrm{b}} = \sigma_{\max}^{\mathrm{b}} \sin\alpha + \sigma_{\min}^{\mathrm{b}} \cos\alpha$. If Re E_y^{b} and Im E_y^{b} have different sign, phases between [90°; 180°] will occur. This is what happens at 10 s (Fig. 6) over the block. At 150 s both real and imaginary parts of E_y^{b} are negatives and phases are between [180°; 270°]. In the case of $\rho_{\min}/\rho_{\max} = 20/200$ both real and imaginary parts have values near zero producing very low apparent resistivities over a wide zone around the centre of the block. In the case of $\rho_{\min}/\rho_{\max} = 10/200$ this happens only at two points (one being site 2 in Fig. 1). At 500 s and $\rho_{\min}/\rho_{\max} = 10/200$ both parts of E_y^{b} still have the same (negative) sign and for $\rho_{\min}/\rho_{\max} = 20/200$ they have different signs and therefore phases between [270°; 360°]. Note that there are cases (e.g. $\rho_{\min}/\rho_{\max} = 20/200$) where over a short period interval various changes in the sign between both parts of E_y^{b} occur and, accordingly, the phases traverse across three quadrants in a short period interval producing the highly anomalous behaviour. E_x is also responsible for the reverse orientation of E_y^{b}, and therefore for the change of sign between real and imaginary parts of E_y^{b}.

The responses of a model with an anisotropic block alone (without the anisotropic layer) were calculated and E_x (arising from polarization *yx*) was two orders of magnitude smaller than E_y^{h}. Therefore, the additional shift $(\boldsymbol{\sigma}_{xy}^{\mathrm{b}}/\boldsymbol{\sigma}_{yy}^{\mathrm{b}})E_x$ is negligible, the real and imaginary parts of E_y^{b} do not cross zero and no phases greater than 90° occur. Phases higher than 90°, require the interaction with the anisotropic layer.

The first period influenced by the anisotropic layer depends on the skin depth. For the model of Fig. 1 and considering a four-layered model (e.g. Weaver 1994), with $\rho_{\max}$ for the block and $\rho_{\min}$ for the layer, the skin depth for the *yx* polarization at 1 s is 7.3 km. Increasing the depth of the anisotropic layer the anomalous behaviour of the phases starts at longer periods.

APPLICATION TO FIELD DATA

The above results were applied to a magnetotelluric survey carried out in SW Iberian Variscan terranes (Fig. 7). The profile samples the three main terranes involved in the Variscan collision: South Portuguese Zone (SPZ), Ossa Morena Zone (OMZ) and Central Iberian Zone (CIZ). In the Ossa Morena Zone in particular, phases exceeding 90° in the same mode at sites 13, 15 and 16 were found. These sites are located in the 'Serie Negra' formation where alternating subvertical bands of schists and well-interconnected graphite bearing blackschists crop out (Pous *et al.* 2003), and thus macroanisotropy with a high anisotropic ratio occurs (Bahr 1997; Eisel & Haak 1999).

A dimensionality analysis—using the multisite multiperiod analyses (McNeice & Jones 2001)—for the whole profile indicated a predominant 2-D strike of 105° in the OMZ, the data were rotated accordingly and a preliminary 2-D inversion (Pous *et al.* 2003) of those sites not affected by such anomalous behaviour showed the typical conductive blobs at middle to lower crust, suggesting the presence of a deep anisotropic layer (Heise & Pous 2001). The low resistivity contrast between blobs and host medium indicated a low anisotropy ratio. As sites 13, 15 and 16 were excluded from the inversion, the inverse model did not reveal any shallow conductor beneath the affected sites despite the high graphite content. These sites show the same typical behaviour of the phases and resistivities as that observed in the data responses of the synthetic anisotropic model. The phases exceeding 90° correspond to the TM mode for a coordinate system with strike 105°. Accordingly, we proceeded to include these anisotropy features in the 2-D inversion model.

After trial-and-error modelling we found the model of Fig. 8, which is a simplification of the 2-D inversion model and incorporates azimuthal anisotropic shallow blocks, one beneath site 13 and another beneath sites 15 and 16, as well as a deep anisotropic layer of about 100 km width along the entire Ossa Morena Zone at middle to lower crustal depths. Note that this layer already appeared in the 2-D isotropic inversion model as a sequence of conductive blobs. Accordingly, the model of Fig. 8 still fits the data reasonably well along the entire profile. Both shallow anisotropic blocks have a ratio of 5/5000 Ω m and an anisotropy strike of N130° (25° with respect to the 105° of the 2-D isotropic strike). The anisotropic layer has an anisotropy ratio of 15/50 Ω m and an anisotropic strike of N245° (140° with respect to the 105° 2-D strike). The responses for the four components of the phases (in the coordinate system of the 2-D isotropic strike direction) at these anomalous sites are shown in Fig. 8. From the study conducted previously, we know that there is an ambiguity in the determination of the model parameters despite the fitting of the four components of the impedance tensor. The reasons for the choice of each model parameter are discussed below.

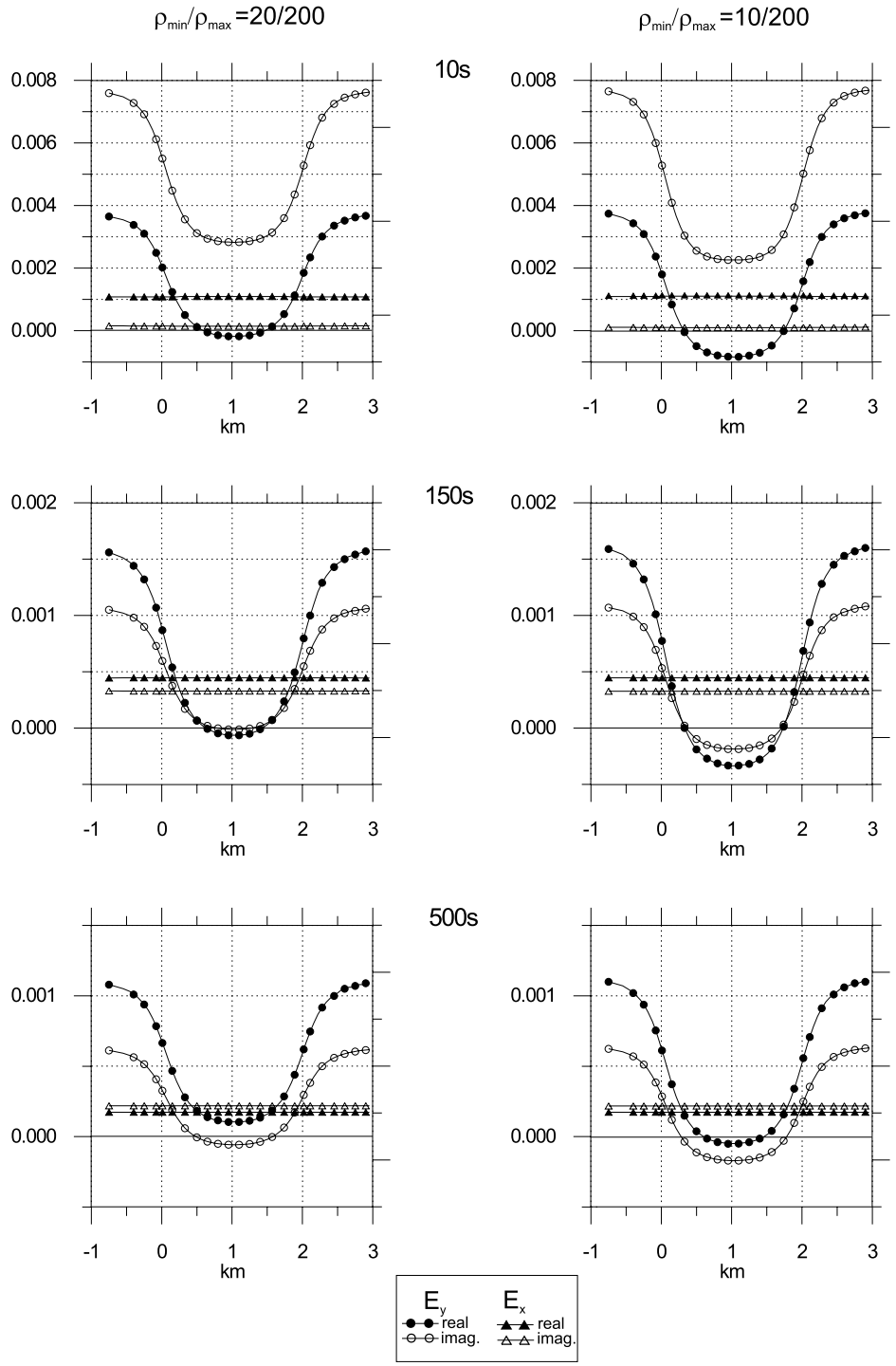

Figure 6. Electric field components for a primary magnetic field in the $-x$ direction above the anisotropic block (located between 0 and 2 km). The plots show E_x and E_y components for the models with $\rho_{\min}/\rho_{\max} = 10/200$ and $20/200$ at 10, 150 and 500 s.

Anisotropy strikes (layer and block)

For a rotation between 130° and 150° the TM phases of sites 15 and 16 do not leave the quadrant. This therefore constitutes a criterion for choosing this angle interval as the anisotropy direction of the block. This angle interval coincided with the *in situ* measured angle of the alternate outcropping blocks of schists and graphite-rich blackschists, which gave a dispersion between 100° and 130° (depending on the sample). We finally chose N130° (25° with respect to the 2-D strike). For the anisotropy layer we just chose N245° (140° with respect to the 2-D strike). This direction fitted the four components of the tensor at sites 13, 15 and 16 (Fig. 8). Small variations of the anisotropy strike increased the misfit.

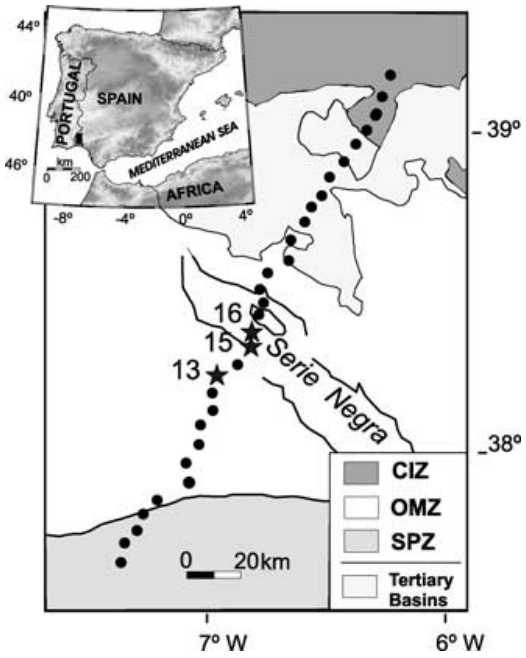

Figure 7. Geological map of the e area showing the locations of the MT sites along the profile. SPZ, South Portuguese Zone; OMZ, Ossa Morena Zone; CIZ, Central Iberian Zone. Stars denote MT sites with phases higher than 90°.

Anisotropy ratio of layer and block

The preliminary 2-D isotropic inversion model (Pous *et al.* 2003) showed evidence of weak anisotropy (conductive blobs of about 10 Ω m in a 50 Ω m background). Accordingly, we chose a ratio of 15/50 Ω m for the anisotropic layer. Because of this low anisotropy ratio (<5), the anisotropy of the layer has only a small influence on the data and on the strike direction analyses (Heise & Pous 2001). Taking into account this low anisotropy ratio of the layer, the ratio of the blocks must be high to produce phases higher than 90°. Moreover, a high anisotropy ratio of the block should be considered given the strong macroanisotropy in the Serie Negra formation. A good data fit was obtained with an anisotropy ratio of 5/5000 Ω m for the blocks. The high value of 5000 Ω m for $\rho_{\max}$ of the blocks was mainly required to fit the *xy* phases.

Geometry of the blocks and layer

The depth, thickness and extension of the anisotropic layer were taken from the inversion model. The lateral extension coincides with the limits of the Ossa Morena Zone. The depth of the layer coincides with the thickness of the zone of conductive blobs in the inversion model. The width of the blocks is restricted by the distribution of the sites with phases exceeding 90°. Note that this effect was restricted to only three sites and from the above synthetic study we consider it as a local phenomenon. The final widths (Fig. 8) of both blocks gave a good data fit. The distance of the sites from the boundaries is a sensitive parameter for fitting the anomalous phases. In contrast, the thicknesses are less constrained. The model depicted in Fig. 8 has the minimum thickness of the blocks required to produce phases higher than 90°.

We analysed the influence of the anisotropic layer, a regional feature, by performing a dimensionality analyses on the synthetic responses of the anisotropic model. The strike analysis applied to the synthetic impedances was carried out using the multisite-multifrequency code of McNeice & Jones (2001). If we consider a data error of 5 per cent the isotropic 2-D strike of 105° could be recovered in a period interval of 7–1000 s within the limits of the confidence interval. This is a consequence of the low anisotropy ratio of the layer. Otherwise, for a high anisotropy ratio of the layer the dimensionality analysis would give the anisotropy strike of the layer as the 2-D regional strike (Heise & Pous 2001). Anisotropy is revealed by the presence of blobs in the 2-D inversion model and from its requirement to fit the anomalous phases at sites above the shallow anisotropic blocks. The sites above the block were not considered in the dimensionality analysis to find the common strike. At these sites the shear angles of the decomposition gave values near ±45°, indicating a three-dimensionality and that the regional impedances cannot be recovered.

CONCLUSIONS

Phases higher than 90° were modelled by combining a deep anisotropic layer and a shallow anisotropic block. We varied the values of the model parameters so as to study the changes in response, and we conclude that, for this particular model, phases out of quadrant occur when:

(1) the anisotropy ratio is high (block and/or layer);
(2) the host medium is high resistive compared with the maximum resistivity of the anisotropic block (from eq. 2);
(3) the angle between anisotropy strikes (of block and layer) is great. The maximum effect is obtained when the angle between both anisotropy strikes is 90°;
(4) the anisotropy strikes differ from the 2-D isotropic strike direction. The maximum effect depends on the particular model parameters given the relationship of eq. (2). In our model of Fig. 1 the maximum effect occurs at $\alpha = 40°$, while the layer has an anisotropy strike of 90° with respect to that of the block;
(5) the block is near the surface and is relatively narrow, not necessarily having to be connected to the layer.

An important consequence of this last point is that for this particular model the anomalous phase behaviour is restricted to sites above the narrow block, and therefore it does not influence the responses of the regional structure significantly. If the anisotropy ratio of the layer was high the dimensionality analyses would give the anisotropy strike as the 2-D strike and the 2-D inversion model would give the 2-D structure projected to the direction of the anisotropy (Heise & Pous 2001). Accordingly, when a few sites in an MT survey appear with phases higher than 90° and there is evidence of anisotropy, these anomalous data can be excluded from the 2-D inversion procedure without significant loss of information when the target is the discovery of regional deeper conductivity structures. There can be cases when the anomalous phases appear extensively in most of the sites and therefore they could respond to a regional feature (e.g. Jones 1993), in which case other explanations should be required (Jones *et al.* 1993).

This procedure was applied to an MT survey in the Ossa Morena Zone where it was possible to include such anisotropic features in an existing isotropic 2-D model and to fit the anomalous phases that appeared at a few sites. The anisotropy ratio of the anisotropic layer was low and the anisotropy had little influence on those sites at a distance of the shallow anisotropic blocks. The high anisotropic ratio of the shallow blocks fitted the data and was consistent with the macroanisotropy associated with the alternate bands of schists and graphite-rich blackschists in the Serie Negra formation. We

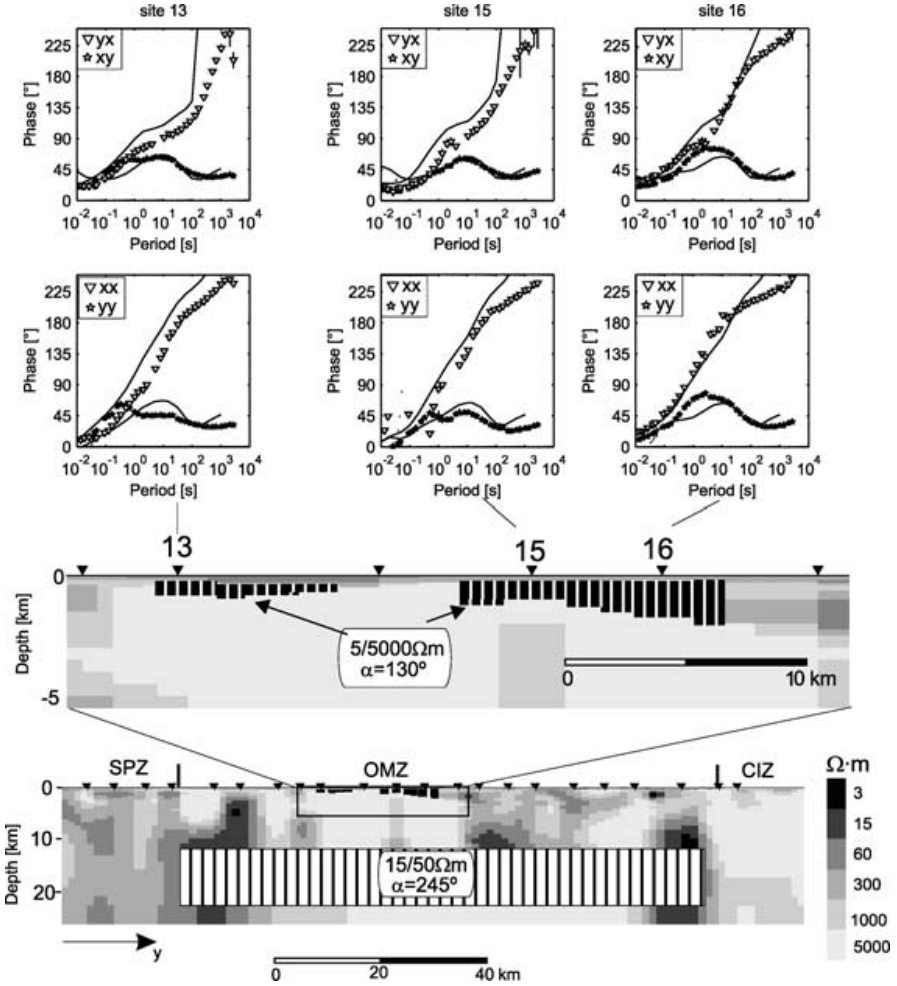

Figure 8. The 2-D inversion (2-D strike =105°) model incorporating the azimuthal anisotropic features: the middle to lower crust of the Ossa Morena Zone was modelled as an anisotropic layer of 15/50 Ω m and an anisotropic strike of 245°. Two anisotropic blocks of 5/5000 Ω m with an anisotropy strike of 130° were added to the upper crust. Upper panel, responses (solid line) and data of the sites with anomalous phases.

showed that the anomalous phases could be reproduced with shallow anisotropic anomalies without affecting the large-scale 2-D model significantly. Moreover, the regional isotropic structure could be recovered in the 2-D inversion when excluding the sites that had phases greater than 90°. Thus, with the anisotropic modelling of the phases higher than 90° we were able to detect the high content of well-connected graphite of the Serie Negra formation, which is evident from field observations.

ACKNOWLEDGMENTS

We thank Josef Pek for his advice in many parts of this manuscript. We also thank Pamela Lezaeta and Alan Jones for their useful comments and recommendations, which helped to improve the manuscript. This study was supported by MCYT of Spain project BTE2000-0583-C02-02.

REFERENCES

Bahr, K., 1997. Electrical anisotropy and conductivity distribution functions of fractal random networks and of the crust: the scale effect of connectivity, *Geophys. J. Int.,* **130,** 649–660.

Berdichevsky, M.N., 1999. Marginal notes on magnetotellurics, *Surveys Geophys.,* **20,** 341–375.

Eisel, M. & Haak, V., 1999. Macro-anisotropy of the electrical conductivity of the crust: a magnetotelluric study from the German Continental Deep Drilling site (KTB), *Geophys. J. Int.,* **136,** 109–122.

Egbert, G.D., 1990. Comments on 'Concerning dispersion relations for the magnetotelluric impedance tensor' eds Yee, E. & Paulson, K.V., *Geophys. J. Int.,* **102,** 1–8.

EMSLAB Group, 1988. The EMSLAB electromagnetic sounding experiment, *EOS, Trans. Am. geophys. Un.,* **69,** 89–91.

Heise, W. & Pous, J., 2001. Effects of the anisotropy on two dimensional inversion procedure, *Geophys. J. Int.,* **147,** 610–622.

Jones, A., 1993. The BC87 Data set: tectonic setting, previous EM results, and recorded MT data, *J. Geomag. Geoelectr.,* **45,** 1089–1105.

Jones, A.G., Groom, R.D. & Kurtz, R.D., 1993. *Decomposition* and modelling of the BC87 dataset, *J. Geomag. Geoelectr.,* **45,** 1127–1150.

Lezaeta, P., 2001. Distortion analysis and 3-D modelling of magnetotelluric data in the Southern Central Andes, *PhD thesis,* Inst. für Geol. Geoph. und Geoinform., Freie Universität Berlin.

Livelybrooks, D., Mareschal, M., Blais, E. & Smith, J.T., 1996. Magnetotelluric delineation of the Trillabelle massive sulfide body in Sudbury, Ontario, *Geophysics,* **61,** 971–986.

McNeice, G.W. & Jones, A.G., 2001. Multisite, multifrequency tensor decomposition of magnetotelluric data, *Geophysics,* **66,** 158–173.

Pek, J. & Verner, T., 1997. Finite difference modelling of magnetotelluric fields in 2-D anisotropic media, *Geophys. J. Int.,* **128,** 505–521.

Pous, J., Heise, W., Schnegg, P., Muñoz, G., Martí, J. & Soriano, C., 2002. Magnetotelluric study of the Las Cañadas Caldera (Tenerife, Canary Islands): structural and hydrogeological implications, *Earth planet. Sci. Lett.,* **204,** 249–263.

Pous, J., Muñoz, G., Heise, W., Melgarejo, J.C. & Quesada, C., 2003. Electromagnetic imaging of Variscan crustal structures in SW Iberia: the role of interconnected graphite, *Earth planet Sci. Lett.,* submitted.

Weaver, J.T., 1994. *Mathematical Methods for Geo-Electromagnetic Induction,* Wiley, New York.

Weckmann, U., 2002. Entwicklung eines Verfahrens zur Abbildung krustaler Leitfähigkeits-strukturen anhand der Magnetotellurikdaten aus Namibia, *PhD thesis,* Inst. für Geol. Geoph. und Geoinform., Freie Universität Berlin.

Weidelt, P., 1999. 3-D conductivity models: implications of electrical anisotropy, in *Three-Dimensional Electromagnetics,* pp. 119–137, eds Oristaglio, M., Spies, B. & Cooper, M.R., Society of Exploration Geophysicists, Tulsa, Okla.